CrossMark

ORIGINAL PAPER

A Comparative Study of the Initial Corrosion of KCl and PbCl$_2$ on a Low-Alloyed Steel

E. Larsson[1] · H. Gruber[1] · K. Hellström[1] ·
T. Jonsson[1] · J. Liske[1] (ID) · J.-E. Svensson[1]

© The Author(s) 2017. This article is an open access publication

Abstract Heat exchange surfaces in biomass- and waste-fired boilers are exposed to corrosive species due to the considerable amounts of alkali chlorides and PbCl$_2$ which are released during combustion. The corrosivity of alkali chlorides toward superheater alloys exposed at high temperature has been studied extensively. However, at lower material temperatures, i.e., at waterwall conditions, considerably less research has been performed. In order to investigate the effect of small amounts of KCl and PbCl$_2$ during the initial stages of the corrosion attack, a Fe–2.25Cr–1Mo steel was exposed for 24 h in an atmospheres consisting of O$_2$ + H$_2$O + N$_2$ at 400 °C. Both KCl and PbCl$_2$ resulted in an increased corrosion rate compared to the reference. The aim of the present paper is to investigate the influence of KCl and PbCl$_2$ on the initial oxidation of a Fe–2.25Cr–1Mo steel. The work involves a detailed microstructural investigation as well as thermodynamic equilibrium calculations.

Keywords KCl · PbCl$_2$ · Waterwalls · Waste combustion · Low-alloyed steel

✉ J. Liske
jesper.liske@chalmers.se

E. Larsson
erik.larsson@chalmers.se

T. Jonsson
torbjorn.jonsson@chalmers.se

J.-E. Svensson
jes@chalmers.se

1   Department of Chemistry and Chemical Engineering, Environmental Inorganic Chemistry, High Temperature Corrosion Center, Chalmers University of Technology, 41296 Göteborg, Sweden

🖄 Springer

Introduction

The fireside environment in biomass- and waste-fired boilers is characterized by high levels of alkali and HCl, which both are believed to cause elevated corrosion rates. To increase the power production from biomass- and waste-fired boilers, it is necessary to increase the steam data of these plants. This increase in steam data implies not only an increase in the material temperature of the superheaters, but also an increase in material temperature of the waterwalls. Low-alloyed steels are often used as waterwall material due to its low cost and mechanical properties. These steels form an oxide scale of Fe_2O_3 and Fe_3O_4 which offer sufficient protection in mildly corrosive environments at moderate temperatures (<500 °C) [1]. At higher temperatures or if the corrosivity of the environment increases, other steel grades and/or coatings are used. In comparison with corrosion of superheaters, the research focused on waterwalls has been scarce. Regarding the corrosion attack of superheaters, where the material temperature is higher, it has been shown by several studies that alkali chlorides are one of the main contributors to the corrosion issues [2–9]. Recent studies have shown that KCl and $PbCl_2$ also accelerates the corrosion rate at the relatively moderate temperatures that exist at the waterwalls [10–13].

Experimental Procedures

Sample Preparation and Analysis

The alloy studied is a Fe–2.25Cr–1Mo steel (also referred to as T22 or 10CrMo910) (see Table 1) for chemical composition. The geometrical area of the sample was 5.56 cm². A hole ($\phi = 1.5$ mm) was drilled for ease of handling. Before exposure, the samples were ground to 320 grit on SiC and polished with three diamond suspensions 9, 3, and 1 μm until the surface appeared mirror-like. The polished samples were degreased and cleaned in acetone and ethanol using ultrasonic agitation.

A tube furnace was used for the exposure, and the temperature was kept at 400 ± 1 °C. The reference atmosphere consisted of N_2 with 5% O_2 and 20% H_2O (g). The salt was deposited on the samples by means of spraying a solution of the desired salt in a 20:80 water/ethanol mixture and subsequently drying with cool air. The amount of salt was applied to result in a weight of 0.1 mg/cm² KCl on the surface. In the case of $PbCl_2$, 0.185 mg/cm² was applied to get equal amounts of Cl in the two cases. Reference samples, without any KCl or $PbCl_2$, were also

Table 1 Chemical composition of the alloy in weight %

Alloy	Fe	Cr	Mo	Mn	Si	C
Fe–2.25Cr–1Mo	Bal	2.2	0.9	0.5	0.3	0.09

investigated. The samples were positioned parallel to the direction of the gas flow, in the center of the furnace. All parts of the system were kept above the dew point of water corresponding to 20% H_2O vapor to prevent condensation. Prior to and after exposure, the samples were stored in desiccators over a drying agent of P_2O_5(s).

Scanning Electron Microscopy (SEM) and Energy-Dispersive X-ray (EDX)

The samples were characterized using a FEI Quanta ESEM 200, equipped with a field emission gun. The microscope was operated in high vacuum mode. The instrument has an Oxford Inca energy-dispersive X-ray (EDX) system for chemical analysis. The acceleration voltage was between 8 and 15 kV for imaging and 15 kV for EDX analysis. Backscattered electrons were used for imaging.

Broad Ion Beam (BIB)

A LeicaTIC3X was used for cross section preparation of exposed samples. A 0.5-mm-thick silicon wafer was glued to the sample with Loctite® 415. The sample was cut with a low-speed saw without lubrication. The three ion guns were operated at 6.5 kV for a duration of 6 h. The attained cross section is approximately 500–1000 μm in width.

X-ray Diffraction (XRD)

A Siemens D5000 powder diffractometer was used to determine crystalline phases present after exposure. The instrument was equipped with a grazing incidence beam attachment together with a Göbel mirror. Cu K_a radiation ($\lambda = 1.52418$ Å) was used with an angle of incidence 0.5°–2°. The measurement range was $10° < 2\theta < 65°$.

Phase diagrams

The thermodynamic calculations were performed using the software FactSage 6.4 and databases: Fact53, ELEM and BINS.

Results and Discussion

Gravimetry

After 24 h of exposure at 400 °C without chloride salts, the mass gain of the Fe–2.25Cr–1Mo is relatively low (see Fig. 1). The presence of KCl increases the corrosion rate substantially with a mass gain of approximately 0.9 mg/cm^2 after 24 h. In the presence of $PbCl_2$, the mass gain (0.62 mg/cm^2) after 24 h is high compared to the reference, but lower than that of the samples exposed in the presence of KCl. This indicates that in these exposure conditions, KCl is more corrosive of the two salts.
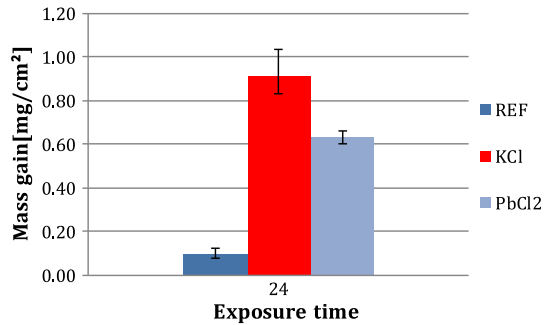
Morphology and Surface Analysis

In the reference case without the presence of chloride salts, the steel has formed a homogenous and smooth oxide all over the surface (see Fig. 2a). In the presence of KCl, the corrosion morphology of Fe–2.25Cr–1Mo is drastically altered (see Fig. 2b). The morphology is characterized by an undulating oxide with KCl particles being partly or fully overgrown by the oxide. Furthermore, the corrosion attack does not seem to be localized to the vicinity of KCl particles. The severe attack of the area between particles, i.e., no KCl present prior to exposure, indicates a fast transport of ions over the surface. The KCl-exposed sample also shows signs of crack formation. The corresponding exposure of Fe–2.25Cr–1Mo in the presence of PbCl$_2$ results in a quite different morphology compared to KCl (see Fig. 2c). The deposited PbCl$_2$ particles have after 24-h exposure completely reacted into PbO, which is seen as the bright areas in the image. This is in line with the XRD analysis in Table 2 showing no diffraction of PbCl$_2$, whereas PbO is detected. Contrary to the samples exposed in the presence of KCl, the corrosion attack of the samples with PbCl$_2$ is more localized to the vicinity of the Pb-containing structures. The XRD analysis in Table 2 shows that KCl is still present after exposure. Furthermore, Fe$_2$O$_3$ and Fe$_3$O$_4$ were detected on all samples.
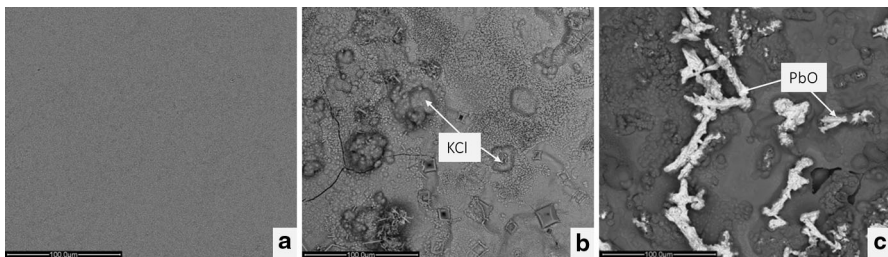

Fig. 2 BSE plan view images of Fe–2.25Cr–1Mo after exposure to 5%O$_2$ + 20%H$_2$O + N$_2$ for 24 h **a** without chloride salt; **b** in the presence of KCl; **c** in the presence of PbCl$_2$

Table 2 XRD analysis of exposed samples, X = detected

	KCl	PbCl$_2$	PbO	Fe$_2$O$_3$	Fe$_3$O$_4$
Ref	–	–	–	X	X
KCl	X	–	–	X	X
PbCl$_2$	–	–	X	X	X

Scale Microstructure After Exposure

In the reference case, a thin and well-adhered oxide has formed on the Fe–2.25Cr–1Mo (see the BIB cross section in Fig. 3). The oxide scale consists of a Fe-rich outward-growing part and an inward-growing part that contains Cr and Fe. The total thickness of the scale is approximately 1 μm. As indicated by the XRD analysis, the scale is a mixture of M$_3$O$_4$ and Fe$_2$O$_3$. The Cr marks the initial surface before exposure, since the diffusion of Cr in M$_3$O$_4$-type oxides is considerably slower compared to Fe [14]. The Cr at the surface is tied up in the M$_3$O$_4$, thereby marking the interface between outward-/inward-growing oxide.

The undulating morphology seen in plan view SEM analysis for the KCl-exposed sample in Fig. 2b is confirmed by the BIB cross section in Fig. 4. The sample exposed to KCl exhibits a layered oxide with numerous voids and poorly attached oxide scales. This type of morphology has recently been reported to be due to KCl particles being consumed, leaving a void behind [15]. The corrosion attack in KCl is rather general, and there is no clear correlation between the original location of the KCl particles and the corrosion attack. The uniform attack indicates a fast surface transport. This may be explained by the formation of a thin liquid film of an eutectic melt in the FeCl$_2$–KCl system, as proposed by [15]. In the present study, there are not any signs of this thin film (see Fig. 4). However, due to the poor resolution of the SEM/EDX analysis and the progress of the corrosion attack, it is not expected to detect this liquid film. Further analysis with, for example, TEM would be needed. In
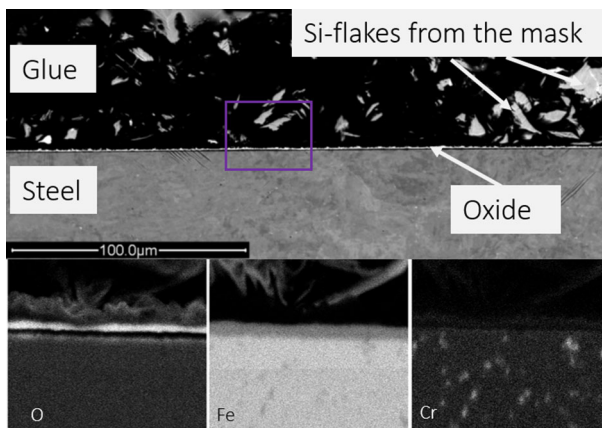

Fig. 3 BIB cross section and EDX mapping of Fe–2.25Cr–1Mo after exposure to 5% O$_2$ + 20% H$_2$O + N$_2$ for 24 h without salt

contrast, traces of subscale metal chlorides can be seen in the EDX analysis in Fig. 4. The porous and non-adherent oxide scales formed on Fe–2.25Cr–1Mo are expected to possess rather poor protection for further oxidation.

According to gravimetry, the mass gain of the sample exposed to $PbCl_2$ was only about 70% of the mass gain of the KCl-exposed sample, indicating a slightly less corrosive environment. The BIB cross section of Fe–2.25Cr–1Mo exposed in the presence of $PbCl_2$ is shown in Fig. 5. Compared to the KCl-exposed samples, the appearance of the oxide scale is significantly different. Instead of a widespread attack all over the surface, as in the case with KCl, the presence of $PbCl_2$ induces a rather localized attack. The thickest oxide scale is located underneath and in the vicinity of an original salt particle. The cross section shows an area of the sample where the $PbCl_2$ was located prior to exposure. The original $PbCl_2$ particle has reacted into PbO, as can be seen in the Pb and Cl EDX maps where no correlation is detected. The fast conversion of $PbCl_2$ into PbO results in a rapid release of chlorine
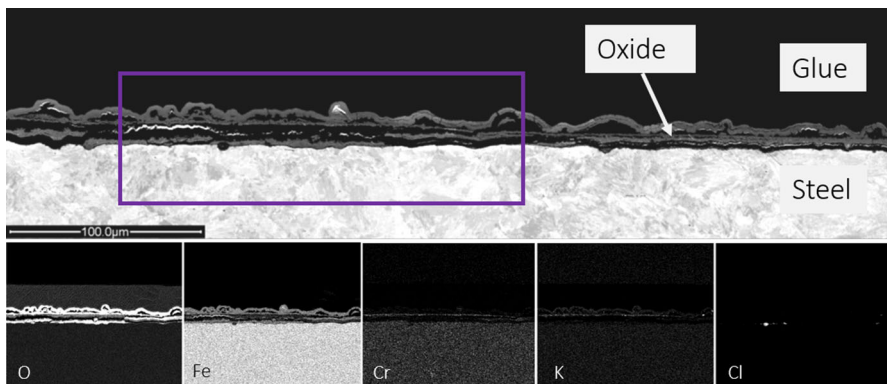

Fig. 4 BIB cross section and EDX mapping of Fe–2.25Cr–1Mo after exposure to 5% O_2 + 20% H_2O + N_2 for 24 h in the presence of KCl

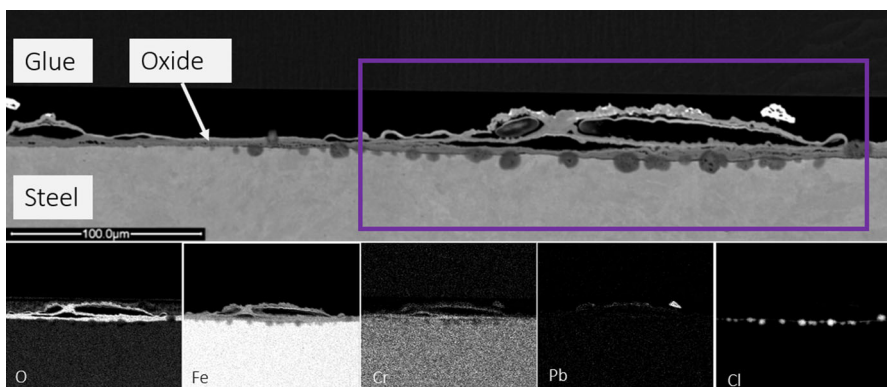Fig. 5 BIB cross section and EDX mapping of Fe–2.25Cr–1Mo after exposure to 5% O_2 + 20% H_2O + N_2 for 24 h in the presence of $PbCl_2$
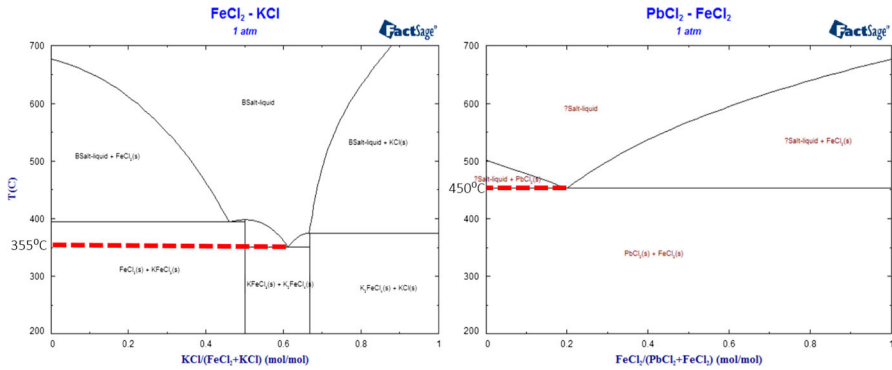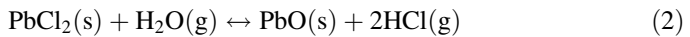
Fig. 6 Phase diagrams of the FeCl$_2$–KCl and FeCl$_2$–PbCl$_2$ system calculated with FactSage

which has penetrated the scale and is located as metal chlorides at the steel/scale interface. Another reason for the localized attack may be that the eutectic temperature for the FeCl$_2$–PbCl$_2$ system (450 °C) is above the exposure temperature which would prevent spreading of the salt (see Fig. 6). Despite the comparably greater presence of subscale metal chlorides in the PbCl$_2$ exposure compared to the KCl exposure, the oxide scale on the PbCl$_2$ seems to be more adherent and dense. However, this may be an effect of the different progress of the corrosion attack in the two cases; for KCl, the subscale metal chlorides may have been evaporated, causing the porous scale, whereas for PbCl$_2$, the corrosion attack has not yet advanced to this stage. The fast reaction of PbCl$_2$ to PbO may in addition explain the less severe attack in the presence of PbCl$_2$ compared to Fe–2.25Cr–1Mo exposed in the presence of KCl, where KCl remains on the surface for a longer duration, see reactions 1–4.

$$KCl(s) + H_2O(g) \leftrightarrow KOH + HCl(g) \tag{1}$$
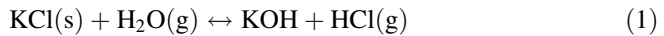
$p(HCl) = 1.1*10^{-10}$ atm at 400 °C calculated with FactSage

$$PbCl_2(s) + H_2O(g) \leftrightarrow PbO(s) + 2HCl(g) \tag{2}$$

$p(HCl) = 1.5*10^{-5}$ atm at 400 °C calculated with FactSage

$$KCl(s) \rightarrow KCl(g) \tag{3}$$

$p(KCl) = 5.4*10^{-10}$ atm at 400 °C, calculated with FactSage

$$PbCl_2(s) \rightarrow PbCl_2(g) \tag{4}$$

$p(PbCl_2) = 5.7*10^{-6}$ atm at 400 °C, calculated with FactSage

Conclusions

The initiation of the corrosion attack of Fe–2.25Cr–1Mo is very rapid under the furnace waterwall conditions in this study.

- The presence of KCl and $PbCl_2$ both increased the corrosion rate on Fe–2.25Cr–1Mo compared to the reference (in the absence of salt) after 24 h of exposure at 400 °C.
- Exposure of Fe–2.25Cr–1Mo in the presence of KCl resulted in a widespread corrosion attack, which partially can be attributed to the presence of a eutectic composition in the $FeCl_2$–KCl system, resulting in a concentration gradient which spreads KCl over the surface.
- Exposure of Fe–2.25Cr–1Mo in the presence of $PbCl_2$ resulted in a localized corrosion attack due to fast decomposition of $PbCl_2$ with a simultaneous release of chlorine. The localized nature of the attack can be attributed to the fast decomposition of $PbCl_2$ into PbO, and also the exposure temperature is below the eutectic temperature in the $FeCl_2$–$PbCl_2$ system which leads to a local release of chlorine.

References

1. P. Kofstad, *High temperature corrosion*, (Elsevier Applied Science, London, 1988).
2. J. Lehmusto, B. J. Skrifvars, P. Yrjas and M. Hupa, Comparison of potassium chloride and potassium carbonate with respect to their tendency to cause high temperature corrosion of stainless 304L steel. *Fuel Processing Technology* **105**, 98 (2013).
3. J. Pettersson, C. Pettersson, H. Asteman, J. E. Svensson and L. G. Johansson, A pilot plant study of the effect of alkali salts on initial stages of the high temperature corrosion of alloy 304L. *Material Science Forum* **461–464**, 965 (2004).
4. J. Pettersson, H. Asteman, J.-E. Svensson and L.-G. Johansson, KCl induced corrosion of a 304-type austenitic stainless steel at 600 °C; the role of potassium. *Oxidation of Metals* **64**, 23 (2005).
5. S. Karlsson, J. Pettersson, L.-G. Johansson and J.-E. Svensson, Alkali induced high temperature corrosion of stainless steel: the influence of NaCl, KCl and CaCl2. *Oxidation of Metals* **78**, 83 (2012).
6. J. Pettersson, C. Pettersson, N. Folkeson, L.-G. Johansson, E. Skog and J.-E. Svensson, The influence of sulphur additions on the corrosive environment in a waste-fired CFB boiler. *Materials Science Forum* **522–523**, 563 (2006).
7. H. P. Nielsen, F. J. Frandsen, K. Dam-Johansen and L. L. Baxter, The implications of chlorine-associated corrosion on the operation of biomass-fired boilers. *Progress in Energy and Combustion Science* **26**, 283 (2000).
8. S. C. Cha and M. Spiegel, Local reactions of KCl particles with iron, nickel and chromium surfaces. *Materials and Corrosion* **57**, 159 (2006).
9. A. Zahs, M. Spiegel and H. J. Grabke, Chloridation and oxidation of iron, chromium, nickel and their alloys in chloridizing and oxidizing atmospheres at 400–700 °C. *Corrosion Science* **42**, 1093 (2000).
10. N. Folkeson, T. Jonsson, M. Halvarsson, L.-G. Johansson, J.-E. Svensson, The influence of small amounts of KCl(s) on the high temperature corrosion of a Fe-2.25Cr-1Mo steel at 400 and 500°C. *Materials and Corrosion* **62**, 606 (2011).
11. S. Enestam, D. Bankiewicz, J. Tuiremo, K. Makela and M. Hupa, Are NaCl and KCl equally corrosive on superheater materials of steam boilers? *Fuel* **104**, 294 (2013).
12. D. Bankiewicz, P. Yrjas, D. Lindberg and M. Hupa, Determination of the corrosivity of Pb-containing salt mixtures. *Corrosion Science* **66**, 225 (2013).
13. D. Bankiewicz, S. Enestam, P. Yrjas and M. Hupa, Experimental studies of Zn and Pb induced high temperature corrosion of two commercial boiler steels. *Fuel Processing Technology* **105**, 89 (2013).

14. J. Topfer, S. Aggarwal and R. Dieckmann, Point-defects and cation tracer diffusion in (CrxFe1-x)(3-δ)O-4 spinels. *Solid State Ionics* **81**, 251 (1995).

15. T. Jonsson, T. Folkeson, J.-E. Svensson and L.-G. Johansson, An ESEM in situ investigation of initial stages of the KCl induced high temperature corrosion of a Fe-2.25Cr-1Mo steel at 400°C. *Corrosion Science* **53**, 2233 (2011).